www.rericjournal.ait.ac.th

Performance Analysis of a Metal Hydride Based Heat Transformer

B. Satya Sekhar* and P. Muthukumar*[1]

Abstract – *A thermal model for predicting the performance of a single-stage metal hydride based heat transformer (MHHT) is presented. The pair of metal hydrides chosen for the present study is $LaNi_{4.7}Al_{0.3}$ and $LaNi_5$.The performance of the system is predicted by solving the combined energy and mass (heat and hydrogen) transfer equations during absorption and desorption of hydrogen to/from the hydride bed in cylindrical coordinates. Numerical results are compared with the experimental data reported in the literature, and a good agreement is found between them. The effects of operating temperatures such as heat source (T_M), heat output (T_H) and heat rejection (T_L) temperatures on the system performances in terms of coefficient of performance (COP_{HT}), specific heating power (SHP) and second law efficiency (η_E) are investigated. For the given range of operating parameters, there exist the optimum values of bed thickness and bed effective thermal conductivity. The COP_{HT} and SHP are found to increase with heat source temperature and however, both are found to decrease with heat output temperature. At the operating conditions of T_H = 423, T_M = 383 K and T_L = 303 K, the COP_{HT} and SHP of the MHHT are found to be 0.415 and 46 W/kg of alloy, respectively. Higher T_L yields better η_E while its value is found to be lower at higher T_M.*

Keywords – Coupled heat and mass transfer, Heat transformer, metal hydrides, performance analysis, thermal model.

1. INTRODUCTION

Energy is indispensable for the developing countries, but the fossil energy reserves are depleting gradually. On the other hand, there is a lot of heat from the renewable energy (*e.g.* solar energy, geothermal energy, *etc.*) or waste heat (*e.g.* heat discharged from industries, thermal power plants, *etc.*) left unused due to their relatively low grade. If the temperature can be upgraded, they will be useful again for many applications. Heat transformer is a type of heat pump of great interest from the energy point of view, which upgrades a part of the waste heat input to a higher temperature and rejects the rest at a lower temperature. Waste heat from the industry and the renewable energy sources can be used as heat input to the heat transformers while the upgraded thermal energy delivered by them can be used as heat input for many industrial applications. Heat transformers based on metal hydrides are extremely attractive as they are efficient, offer wide operating temperature ranges and are environmentally safe. Thus, the growing attention has been given to MHHT's for the effective use of industrial waste heat. In spite of the great potential, very little work has been carried out on the metal hydride based heat transformers (MHHT).

Werner and Groll [1] developed a laboratory scale prototype of a two-stage MHHT. Suda *et al.* [2] developed a two-stage MHHT for upgrading heat from 80 °C to 120 °C with a capacity of about 77 kW. The metal hydrides employed were; $LaNi_{4.28}Al_{0.23}$ as low pressure hydride, $MmNi_{4.57}Al_{0.46}Fe_{0.05}$ as intermediate pressure hydride and $MmNi_{3.98}Fe_{1.04}$ as high pressure hydride. Isselhorst and Groll [3] developed a prototype of MHHT with a capacity of about 8 kW using $LmNi_{4.85}Sn_{0.15}$, $LmNi_{4.49}CO_{0.1}$-$Mn_{0.205}Al_{0.205}$ and $LmNi_{4.08}Co_{0.2}Mn_{0.62}$ $Al_{0.1}$. They showed that an upgrading of thermal energy from 130-140 °C to 200 °C with a heat sink temperature of 30- 40 °C could be possible. They reported COP and the specific alloy output were 0.27 and 38 W/kg of total hydride mass, respectively. Willers and Groll [4] built and tested a two-stage MHHT. At the operating temperatures of 190-200 °C for the useful heat, 130-135 °C for the driving heat and 40 °C for the waste heat, the reported maximum COP was about 0.1. Kang and Yabe [5] formulated a reaction front model for predicting the performances of MHHT for upgrading waste heat at 100 °C to 127 °C using $LaNi_5$/$LaNi_{4.5}Al_{0.5}$. Gopal and Murthy [6] numerically studied the performances of a single-stage MHHT working with $ZrCrFe_{1.4}$/$LaNi_5$ using a one-dimensional model. Kumar *et al.* [7] carried out a comparative thermodynamic study of the MHHT and metal hydride based heat pumps for different alloy pairs. The results were presented in the form of nomograms to yield the operation temperatures, COPs, and exergy efficiencies. Sun *et al.* [8] presented a method to select the hydride alloys for two-stage MHHT. George and Murthy [9] conducted experiments on a 3 kW vapor absorption heat transformer to study the influence of operating temperature on its performance. COPs in the range of 0.2 – 0.35 and a heat delivery temperature of 85 °C with the temperature lifts up to 20 °C were achieved. Yang *et al.* [10] developed a 2-D mathematical model to simulate the performance of MHHT. They introduced a new term called "temperature boost" to evaluate the performance of the system [11]. They found that the amount of hydrogen transferred between coupled reactors is crucial to obtain a high COP, while *SHP* is very sensitive to the cycle time. It is seen from the literature that many investigators demonstrated the

*Department of Mechanical Engineering, Indian Institute of Technology Guwahati, Guwahati-781039, India.

[1]Corresponding author; Fax: +91 361 2690762.
E-mail: pmkumar@iitg.ernet.in; pmuthukkumar@yahoo.com.

operation of MHHT prototypes. Unlike the conventional vapour absorption type heat transformer, MHHT can be used for upgrading the heat in the range of about 130-140 °C to 190-220 °C [3]. It is well known that the performance of the MHHT is essentially determined by the heat and mass transfer processes between coupled reaction beds. In order to predict the optimum range of operating temperatures and their effect on the performance parameters, it is essential to study the heat and mass transfer characteristics of the coupled metal hydride beds of the MHHT before planning for an expensive experimental investigation. The thermal models reported by Kang and Yabe [5] and Gopal and Murthy [6] are one dimensional and limited to thin reaction beds. Further, these models did not consider the pressure drop across the reaction bed, the variation in heat transfer fluid temperature along the axial direction of the reactor and the effect of convective heat transfer in the energy equation. Yang *et al.* [10, 11] have not presented the effect of operational parameters on the second law efficiency of MHHT. Hence, in this paper, the authors present a thermal model for predicting the performances of MHHT considering the effects of convective heat transfer in the energy equation and also the variation in the heat transfer fluid temperature along the axial direction of the reactor. The effects of various operating temperatures on the performance of the MHHT in terms of COP_{HT}, *SHP*, cycle time and second law efficiency are presented.

2. PHYSICAL MODEL

Figure 1 shows the design details of the coupled metal hydride reaction beds that consists of a pair of similar metal hydride reactors A and B, filled with $LaNi_5$ and $LaNi_{4.7}Al_{0.3}$ respectively. Each reactor is of 32 mm inner diameter and 500 mm length. The inner most tube of 12 mm outer diameter and 6 mm internal diameter acts as hydrogen filter. It ensures the instantaneous availibility of hydrogen throughout the reaction bed during initial stage of absorption process and also it prevents the hydride particle from being carried away by the hydrogen gas during the desorption process.The reactor wall thickness is taken as 1.0 mm. Metal hydride is filled in the space between the filter and the reactor wall. The heat transfer fluid (HTF) flows around the reactor tube (shown in Figure 1). The two reactors are connected by a tube of 3.0 mm inner diameter (1.5 mm thickness) and 300 mm length with a control valve through which the hydrogen is exchanged freely between the reactors.

The operating principle of a single-stage MHHT on van't Hoff plot is shown in Figure 2. The operating cycle consists of two coupled heat and mass transfer processes (ab and cd) and two sensible heat transfer processes (bc and da). The system operates in three temperature limits viz., heat output (T_H), heat input or driving heat (T_M) and heat rejection (T_L) and two pressure limits (P_H>P_L). Initially, it is assumed that the reactor A is fully hydrided and the reactor B is fully dehydrided at their respective operating temperatures of T_M and T_H. During the process ab, the control volve between A and B is opened. Reactor A starts desorbing the hydrogen by taking the heat at heat source temperature T_M and reactor B starts absorbing the hydrogen by rejecting the heat at T_H (useful output).This process is continued until a pre-determined amount of hydrogen exchange takes place between the reactors A and B. During the second process bc, the valve between the reactors is closed. Reactors A and B are sensibly cooled down to the heat rejection temperature T_L and the heat source temperature T_M, respectively. During the process cd, the valve between the two reactors is opened. Due to the pressure difference between (with respect to their Pressure– Concentration– Temperature characteristics) the hydrides, the reactor B starts desorbing hydrogen by extracting the heat from heat source temperature T_M and the reactor A starts absorbing the hydrogen by rejecting the heat at low temperature T_L. This process is continued until a pre-determined (the same as during the process ab) amount of hydrogen transfer takes place between the reactors B and A. Finally (process da), the valve between the two reactors is closed and the reactors A and B are sensibly heated to the heat source temperature T_M and heat output temperature T_H, respectively, so that the reactors A and B reach their initial conditions and thus the cycle repeats.

3. MATHEMATICAL MODEL

A pair of metal hydrides considered for the present analysis is selected based on the equilibrium conditions at points *a*, *b*, *c* and *d* illustrated in Figure 2 at the heat output, heat input, and heat rejection temperatures. The reaction enthalpy and entropy of the selected metal hydride alloys are listed in Table 1. For simplifying the thermal modeling of the MHHT, the following assumptions are made.

1. The local thermal equilibrium between the hydride bed and hydrogen is valid [13].
2. Due to the moderate temperature, the heat transfer by radiation within the hydride bed is neglected.
3. Hydrogen is assumed as a perfect gas.
4. The thermo-physical properties of hydride alloy are independent of concentration and pressure.
5. The temperature (T_g) and hydrogen gas pressure (P_g) in the combined space are uniform throughout the connecting tube but they are time dependent.
6. Heat transfer between the reactors and the surroundings is neglected.

The hydride equilibrium pressure (P_{eq}) is calculated using the van't Hoff equation [13].

$$P_{eq} = 10^5 \exp\left[\frac{\Delta H}{R_u T} - \frac{\Delta S}{R_u} + (\phi \pm \phi_o)\tan\left[\pi\left(\frac{X}{X_f} - \frac{1}{2}\right)\right] \pm \frac{\beta}{2}\right] \quad (1)$$

where '+' sign is used for hydriding process and '-' used for dehydriding process, and X and X_f are the concentration at the given time (t) and final hydrogen concentration in the hydride bed, respectively.

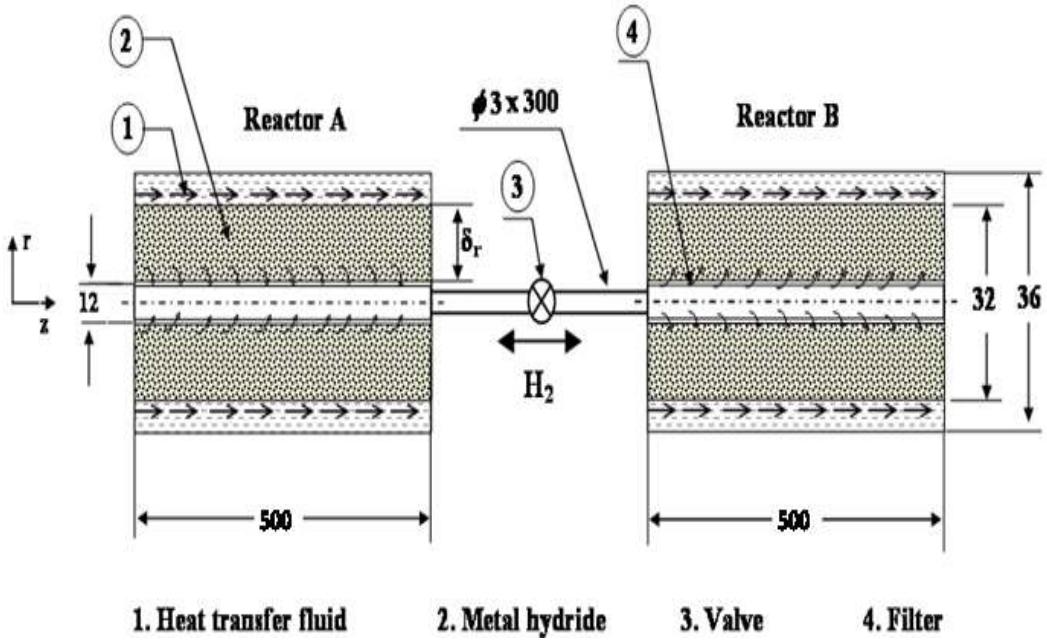

All dimensions are in mm

Fig. 1. Schematic of coupled metal hydride reactors.

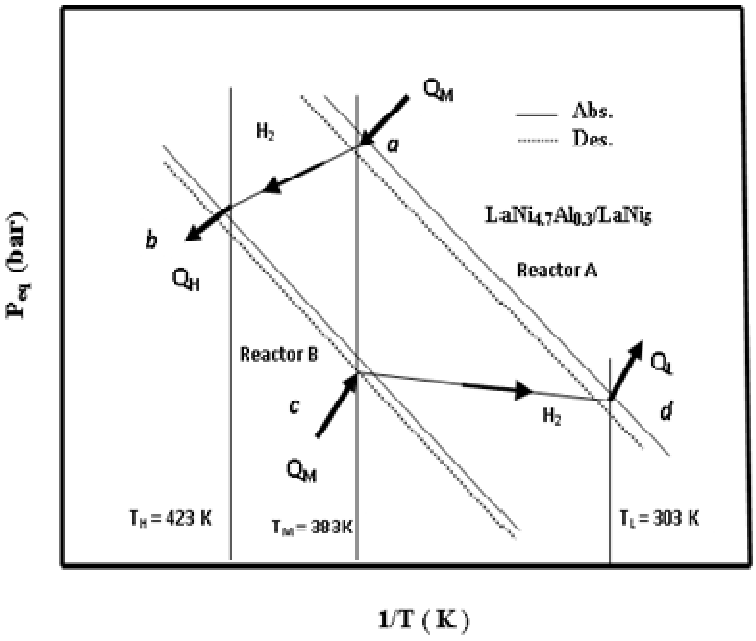

Fig. 2. van't Hoff plot for a single-stage MHHT.

Table 1. Thermo-physical properties of alloys [16].

Alloys	ΔH (kJ/mol H_2)		ΔS (J/mol H_2-K)	
	Abs	Des	Abs	Des
$LaNi_5$	- 28.5	- 30	-103.2	-104.7
$LaNi_{4.7}Al_{0.3}$	-33.9	-34.9	-105	-106.4

The gas pressure and temperature in the combined gas space immediately after opening the valve are calculated from the following expressions;

$$P_{g,P} = \frac{P_{g,A}V_A + P_{g,B}V_B}{V_A + V_B}\ ,\ T_{g,P} = \frac{n_A T_A + n_B T_B}{n_A + n_B} \qquad (2)$$

where, V_A and V_B are the void volumes of the reactors A and B, respectively. The number of moles of hydrogen in the respective reactors n_A and n_B are calculated using the following perfect gas equation;

$$n_A = \frac{P_A V_A}{R_u T_A} \ , \ n_B = \frac{P_B V_B}{R_u T_B} \tag{3}$$

The number of moles of hydrogen (n_g), gas temperature (T_g) and pressure (P_g) in the combined gas space at any time (t+δt) during the hydrogen transfer process are calculated using the following equations;

$$n_{g,t+\delta t} = n_{g,t} + n_d - n_a \tag{4}$$

$$T_{g,t+\delta t} = \frac{\left(n_{g,t} - n_a\right) T_{g,a} + n_d T_{g,d}}{n_{g,t} - n_a + n_d} \tag{5}$$

$$P_{g,t+\delta t} = \frac{n_{g,t+\delta t} R_u T_{g,t+\delta t}}{V_A + V_B + V_P} \tag{6}$$

where, $n_{g,t}$ denotes the number of moles of hydrogen in the connecting tube immediately after opening the valve, and n_a and n_d are the number of moles of hydrogen absorbed by the reactor B and the number of moles of hydrogen desorbed from the reactor A during t = δt.

The rate of hydrogen transferred between the coupled reactors and the heat interaction of the individual reaction beds with heat transfer fluids are predicted by simultaneously solving the continuity, the momentum, and the energy equations of the reactors A and B during the processes ab and cd.

In the following sections, the details of heat and mass transfer processes between the coupled reactors are explained.

3.1. Process ab

During the process ab, hydrogen is desorbed from the reactor A by taking the heat of desorption from the heat transfer fluid temperature at T_M and the same hydrogen is absorbed by the reactor B by releasing the heat of absorption to the heat transfer fluid at upgraded temperature T_H. In the following subsection, the modeling of coupled heat and hydrogen transfer process between the reactors A and B are discussed.

Reactor A (desorption)

Rate of hydrogen (mass flow rate per unit volume) desorption from the reactor A is estimated using following equation [14]

$$m_A = R_d \exp\left(\frac{-A_d}{R_u T_A}\right)\left(\frac{P_{eq,A} - P_{g,t+\delta t}}{P_{eq,A}}\right)\rho_{m,A} \tag{7}$$

where, P_g is the gas pressure in the combined gas space at any given time (Equation 6) and $\rho_{m,A}$ denotes the density of hydride at any given time t.

Due to the assumption of local thermal equilibrium between the hydrogen and the hydride bed, a combined energy equation is considered for predicting the temperature in the reaction bed [15].

$$\left(\rho C_p\right)_e \frac{\partial T}{\partial t} + \left(\rho C_p\right)_g \vec{u}.\nabla T = \lambda_e \nabla^2 T - m_A \left[\frac{\Delta H}{M_g} - T\left(C_{P,g} - C_{P,m}\right)\right] \tag{8}$$

where,

$$\left(\rho C_p\right)_e = \left(\varepsilon \rho C_p\right)_g + \left((1-\varepsilon)\rho C_p\right)_m \tag{9}$$

and the effective thermal conductivity is given by;

$$\lambda_e = \varepsilon \lambda_g + (1-\varepsilon)\lambda_g \tag{10}$$

The hydrogen mass balance is expressed as;

$$\varepsilon \frac{\partial\left(\rho_g\right)}{\partial t} + \nabla\left(\rho_g \vec{u_g}\right) = m_A \tag{11}$$

where ρ_g denotes the density of the hydrogen in the reactor A and it is calculated using the perfect gas law. The velocity of hydrogen gas is determined using the Darcy's law (creeping flow);

$$\vec{u}_g = -\frac{K}{\mu_g} \nabla P_g \ . \tag{12}$$

By substituting the values of u_g and ρ_g in Equation 11, the gas pressures (P_g) inside the reactor at different radial and axial location are calculated using the following equation.

$$\left(\frac{\varepsilon M_g}{R_u T}\right)\frac{\partial P_g}{\partial t} + \left(\frac{\varepsilon M_g P_g}{R_u}\right)\frac{\partial}{\partial t}\left(\frac{1}{T}\right) - \frac{K}{\nu_g r}\frac{\partial}{\partial r}\left(r\frac{\partial P_g}{\partial r}\right) - \frac{K}{\nu_g}\frac{\partial}{\partial z}\left(\frac{\partial P_g}{\partial z}\right) = m_A \ . \tag{13}$$

Initial and Boundary Conditions

Initially at time $t = 0$; the hydride concentration, the temperatures of the hydrogen gas and metal hydride and the density of the metal hydride are assumed to be uniform throughout the reactor bed. They are given by;

$$\rho_{m,A}(z,r) = \rho_{ss} \ ; \quad T_{m,A}(z,r) = T_{g,A}(z,r) = T_M \ ; X_A(z,r) = X_{\max.A} \ . \tag{14}$$

The right and left boundaries of the reactor are considered as adiabatic (well insulated).

$$\frac{\partial T}{\partial z}(z,r,t)_{z=0} = 0 \ ; \ \frac{\partial T}{\partial z}(z,r,t)_{z=Z} = 0 . \tag{15}$$

At the bottom wall (along the porous filter), gas pressure is uniform throughout the length of the reactor;

$$P_g\ (z, r_i, t) = P_g\ . \tag{16}$$

The HTF flows around the reaction bed tube and therefore the convective boundary condition is applied at top boundary r = r_o.

$$-\lambda_e \frac{\partial T}{\partial r}(z, r_O, t) = h\,(T_{z,r_o,t} - T_f) \tag{17}$$

where, T_f and $T_{(z,ro,t)}$ denote the temperatures of the HTF and the hydride bed at the outer radius, respectively. Most of the investigators assumed that the temperature of the HTF is constant along the axial direction [5], [6]. However, in practice, due to the limitation of HTF flow rate, there will be a variation in the HTF temperature along the axial direction and hence, the variable wall temperature convective boundary condition (non-isothermal convective boundary condition) is considered in the present study. The variation in the HTF along the axial direction is updated using the following equation [17].

$$T_{fo} = T_{fi} + [T_{z,r_o,t} - T_{fi}]\left[1 - \exp\left(-\frac{hA}{m_f Cp_f}\right)\right]. \tag{18}$$

Reactor B (Absorption)

The rate of hydrogen absorption by the reactor B is expressed as [14]

$$m_B = R_a \exp\left(\frac{-A_a}{R_u T_B}\right)\ln\left(\frac{P_{g,t+\delta t}}{P_{eq,B}}\right)\left(\rho_{ss} - \rho_{m,B}\right) \tag{19}$$

The hydride equilibrium pressure (P_{eq}) is calculated from Equation 1. The temperature of the reactor B is updated by solving the following energy equation;

$$\left(\rho\, C_p\right)_e \frac{\partial T}{\partial t} + \left(\rho\, C_p\right)_g \vec{u}.\nabla T = \lambda_e \nabla^2 T + m_B\left[\frac{\Delta H}{M_g} - T\left(C_{P,g} - C_{P,m}\right)\right]. \tag{20}$$

The mass balance during absorption of hydrogen in the reactor B is given by;

$$\varepsilon \frac{\partial\left(\rho_g\right)}{\partial t} + \nabla\left(\rho_g \vec{u_g}\right) = -\ m_B\ . \tag{21}$$

Hydrogen gas pressure in the reactor B is calculated in the same way as for the reactor A using Equation 13.

Initial and Boundary Conditions

The initial condition of the reactor B at time t = 0 is given as

$$\rho_{m,B}(z, r) = \rho_i\ ;\quad T_{m,B}(z, r) = T_{g,B}(z, r) = T_H\ ; X_B(z, r) = X_{\min,B}\ . \tag{22}$$

The boundary conditions of reactor B are similar to those for the reactor A. The initial conditions stated above are used only at the first cycle.

Process bc

During this process, the control valve remains closed. Hence, there is no hydrogen transfer between the reactors A and B and only sensible heat exchange takes place between the hydride bed and the heat transfer fluid.

The change in the hydride bed temperature during the sensible cooling process is estimated using the following energy equation. The final condition of process ab is taken as the initial condition of the process bc.

$$\left(\rho\, C_p\right)_e \frac{\partial T}{\partial t} + \left(\rho\, C_p\right)_g \vec{u}.\nabla T = \lambda_e \nabla^2 T\ . \tag{23}$$

3.3. Process cd

During this process, the hydrogen is exchanged from the reactor B to the reactor A at low pressure. The governing equations and boundary conditions used in this process are similar to those for the process ab and however, the boundary temperatures are different [refer section 2]. The final condition of the process bc is taken as the initial condition of the process cd.

3.4. Process da

During this process, the reactors A and B are sensibly heated to T_M and T_H, respectively. Using Equation 23, the temperature of the hydride bed is updated. The final condition of this process is the initial condition of the process ab of second cycle.

3.5. Performance Analysis

The performances of a single-stage MHHT are defined in terms of coefficient of performance (COP_{HT}), specific heating power (SHP) and second law efficiency (η_E). The COP_{HT} is defined as;

$$COP_{HT} = Q_H / Q_M \tag{24}$$

where

$$Q_H = Q_{B,ab} - Q_{B,da} \tag{25}$$

Q_H denotes the heat output obtained at the heat output temperature, T_H. Q_M is the heat input at T_M. $Q_{B,ab}$ and $Q_{B,da}$ are the energy transfers between the heat transfer fluid and the hydride bed B during the processes ab and da, respectively. These quantities are defined as;

$$Q_{B,ab} = n_{B,ab}\Delta H_{B,ab} \tag{26}$$

$$Q_{B,da} = m_B C_{pB}\,(T_H - T_M) \tag{27}$$

where m_B is combined masses of the hydride B and the reactor material. The ratio between hydride mass and the reactor mass is taken as 0.5. The energy supplied at the medium temperature, T_M is given by

$$Q_M = Q_{A,ab} + Q_{A,da} + Q_{B,cd} \tag{28}$$

where, $Q_{A,ab}$, $Q_{B,cd}$and $Q_{A,da}$ are the energy supplied to the reactors A and B during the processes ab, cd and da,

respectively and the respective quantities are defined as follows;

$$Q_{A,ab} = n_{A,ab} \Delta H_{A,ab} \quad (29)$$

$$Q_{B,cd} = n_{B,cd} \Delta H_{B,cd} \quad (30)$$

$$Q_{A,da} = m_A C_{pA} (T_M - T_L) \quad (31)$$

The specific heating power (*SHP*) plays a significant role in the performance of MHHT. It is defined as the net heat output obtained over a cycle per unit mass of alloy.

$$SHP = Q_H / (m_B + m_A) t_{cy} \quad (32)$$

where, m_A and m_B denote the total masses (which include both the masses of the hydride and the reactor material) of the reactor A and B, respectively and t_{cy} denotes the total cycle time.

The second-law efficiency (η_E) measures the performance of the system with reference to its performance under reversible conditions. It is defined as;

$$\eta_E = \frac{COP_{HT}}{COP_{Carnot}} \quad (33)$$

The COP_{Carnot} for single-stage MHHT is defined as

$$COP_{Carnot} = \frac{\left(1 - \frac{T_L}{T_M}\right)}{\left(1 - \frac{T_L}{T_H}\right)} \quad (34)$$

4. NUMERICAL TECHNIQUE

The numerical solution of the present mathematical model is obtained using the fully implicit finite volume method. Initially, the reactors are is in thermal equilibrium and the pressures inside the reactors A and B are calculated using Equation 1. During the process ab (once the valve is opened), the hydrogen is desorbed from the reactor A which is absorbed in the reactor B. This process is allowed till a specific amount of hydrogen is exchanged from the reactor A to the reactor B. The processes ab and cd are assumed to be converged when the difference between the cumulative amount of hydrogen transfer and the predefined amount of hydrogen transfer is less than 0.0001 g. Since, there is no mass transfer during the sensible heat transfer processes, the processes bc and da are assumed to be converged when the difference between the average bed temperature (area average) and the HTF temperature is less than 0.1 K. The end condition of the sensible heating process da is taken as the initial condition of the process ab of the second cycle. The cycle is repeated (minimum 5 cycles) till all the processes reach stable and then the computed values are presented. The grid independence test is carried out for analyzing the effect of total number of grids on the variation of hydride concentration in the reactors A and B with time. As illustrated in Figure 3, a good agreement is observed between the grid sizes 41 x 41 and 51 x 51. Hence, the present analysis is carried out using a minimum grid size of 41 x 41.

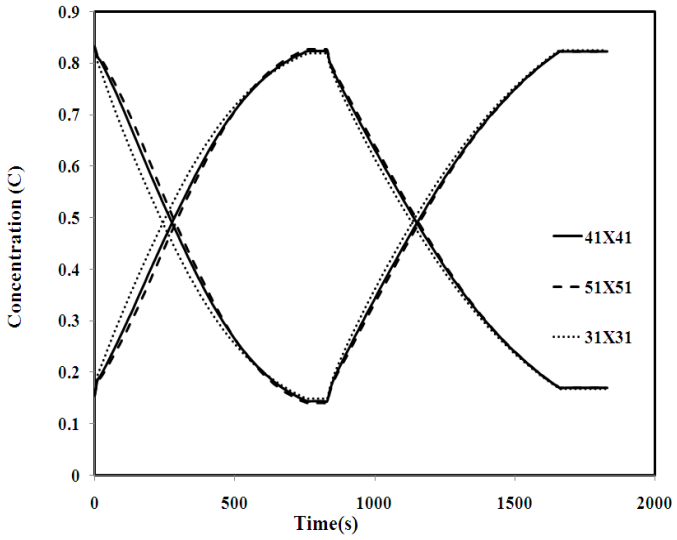

Fig. 3. Grid independent test.

5. RESULTS AND DISCUSSION

In this section, the results obtained from the numerical simulation are presented. The performance of the system is predicted by employing both the convection boundary conditions (isothermal and non-isothermal). The range of operating temperature, properties of hydrogen gas and metal hydride alloys, and the constants used in the present thermal model are presented in Table 2.

5.1 Numerical Validation

Not much experimental works have been reported on a single-stage MHHT. In order to validate our present numerical model, we have compared our numerical results with the experimental results of a single-stage metal hydride based heat pump reported by Ni and Liu [12]. The pair of metal hydrides chosen for the validation is $LaNi_{4.61}Mn_{0.26}Al_{0.13}$ (the high-pressure hydride) and $La_{0.6}Y_{0.4}Ni_{4.8}Mn_{0.2}$ (the low-pressure hydride).

Reactor dimensions and thermo-physical properties of metal hydride alloys used for the validation purpose were taken from Ni and Liu [12]. It is observed from Figure 4 that the predicted regenerative (high temperature) hydride average bed temperature profiles at two heat source temperatures viz., 403 K and 423 K match reasonably well with the experimental data reported by Ni and Liu [12]. For a heat source temperature of 423 K, the maximum deviation of the numerical results from the experimental data is about 3.8 %. In the following sections results obtained for a single-stage MHHT working with $LaNi_{4.7}Al_{0.3}/LaNi_5$ are presented.

Table 2. Design and operating data, properties and constants used for numerical analysis.

Low / High temperature hydride bed	$LaNi_5$/ $LaNi_{4.7}Al_{0.3}$
Low temperature (T_L)	298-313 K
Medium temperature (T_M)	378-393 K
High temperature (T_H)	413-428 K
Specific heat capacity (C_p)	419 J/kg-K
Porosity (ε)	0.5
Mass flow rate of HTF (m_f)	0.01254 kg/s
Bed thickness (r_o-r_i)	0.01 m
Density of solid (ρ_m)	8400 kg/m^3
Properties of hydrogen	
Density of hydrogen (ρ_g)	0.0838 kg/m^3
Specific heat of hydrogen ($C_{p,g}$)	14283 J/kg-K
Thermal conductivity of hydrogen (λ_g)	0.127 W/m-K

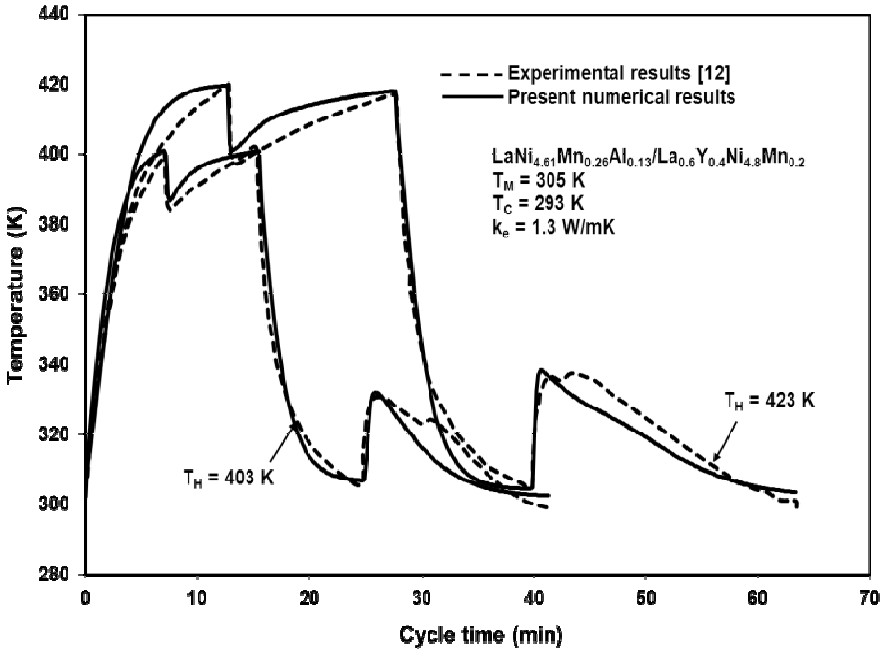

Fig. 4. Validation of predicted hydride bed temperature profiles over a complete cycle.

5.2 Effect of Convective Boundary Conditions on the Variation of Hydride Concentrations

The variations of the hydride concentration in the reactors A and B over a complete cycle are shown in Figure 5. The four processes of the MHHT are respectively indexed as ab, bc, cd and dc. During the processes ab and cd, (hydriding and dehydriding reactions occur respectively in A and B) the hydride concentration in the reactor A varies from 0.83 to 0.15 and in the reactor B varies from 0.15 to 0.83.Though, the same amount of hydrogen is transferred during the processes ab and cd, the time taken during the process ab (760 s) is shorter than that of the process cd (830 s).

This is mainly due to higher pressure difference (higher driving potential) between the equilibrium pressures of the reactor A and B during the processes ab. Since, there are no hydrogen transfer during the processes, bc and da, the time take for these processes are in the order of 2 min. During the process ab, the hydrogen starts desorbing from the reactor A. The HTF enters at the left boundary (z = 0) and leaves from the

reactor at the right boundary (z = 500 mm). Due to the heating of the hydride, there is a significant drop in the HTF temperature when it reaches the right boundary. Hence, the rate of hydrogen desorption at the left boundary is higher in comparison with the right boundary. In case of the isothermal convective boundary condition, the HTF temperature is assumed to constant along the length of the reactor, resulting in uniform hydrogen desorption along length of the reactor. Therefore, the cycle time of the non-isothermal wall convective temperature boundary condition is higher by about 3 min compared to that of the isothermal wall convective temperature boundary condition.

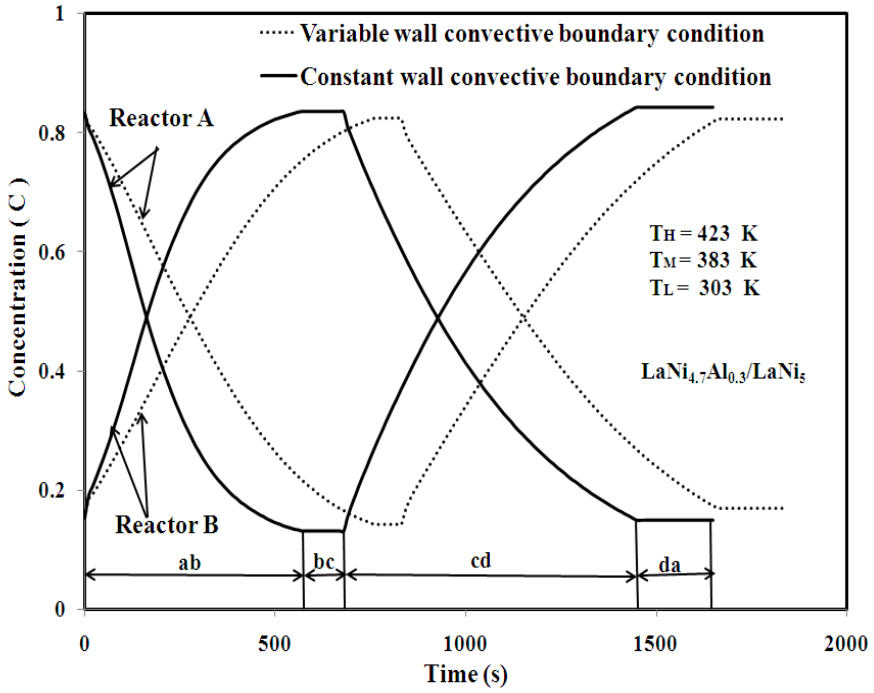

Fig. 5. Effect of convective boundary conditions on average hydride concentrations.

5.3 Variation of Average Hydride Bed Temperature Profiles over a Cycle

The variation of average bed temperature of the reactors A and B over a cycle is illustrated in Figure 6. Due to the low thermal conductivity of hydride bed, the temperature of the absorbing bed increases sharply; while the desorbing bed drops rapidly during the initial stage of the process ab and then approach the HTF temperature gradually at the end of the process ab. The sudden rise/drop in the bed temperature is undesirable as it reduces the driving potential (pressure difference) for the hydrogen transfer between the reactors. The temperature rise/drop depends upon the initial reaction rate, *i.e.*, the equilibrium pressure difference between the hydride beds A and B. It is observed that the initial bed temperature drop/rise in the hydride B is marginally greater than that of the hydride A. This is due to the higher heat of formation of the hydride B than the hydride A.

5.4 Variation of HTF Temperature at Different Axial Locations

The variations in HTF temperature over a cycle at different axial locations are presented in Figure 7. At the beginning of the absorption process (reactor B), the reaction starts rapidly due to large driving potential, resulting in sudden rise in the bed temperature. Owning to a larger temperature difference, the HTF gains more heat from the bed during the initial rapid absorption process. The difference in temperatures between the HTF at the inlet (z ≅ 12 cm) and at the out (z ≅ 47.5 cm) is about 23 K.

Later, this difference decreases gradually due to the fall in reaction rate and it approaches zero at the end of the absorption process. During the desorption process, the HTF temperature at the right boundary is found to be lower than that of the left boundary. When the HTF reaches the right boundary, it loses the heat to the bed, resulting in temperature fall. As explained in Figure 6, due to large heat of formation of the hydride B, the difference in temperatures of the HTF flowing around the reactor B between at z = 12 cm and at z = 47.5 cm is higher than the respective value of the reactor A

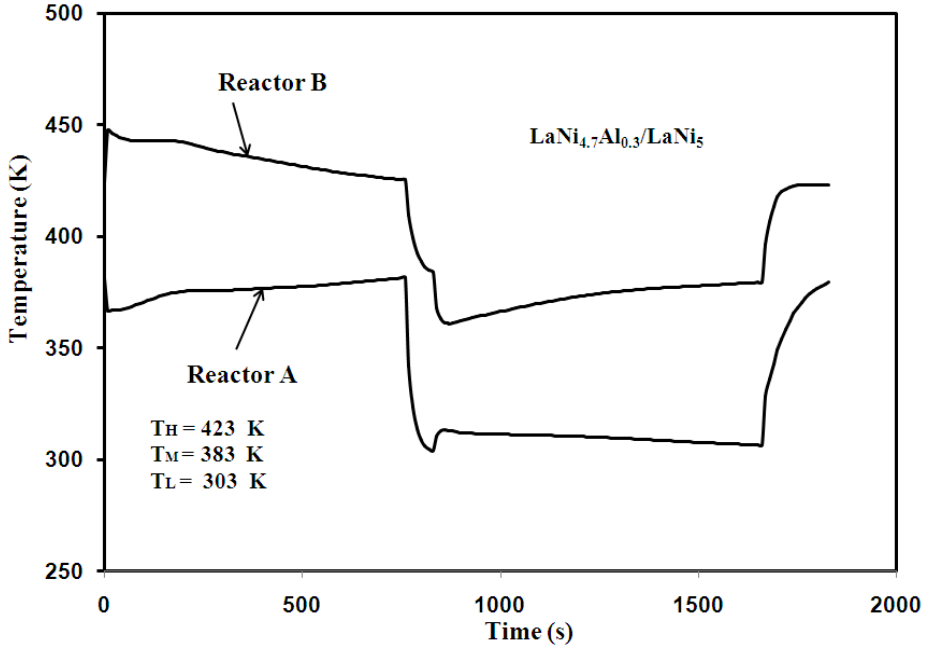

Fig. 6. Variation of average hydride bed temperature profiles over a complete cycle.

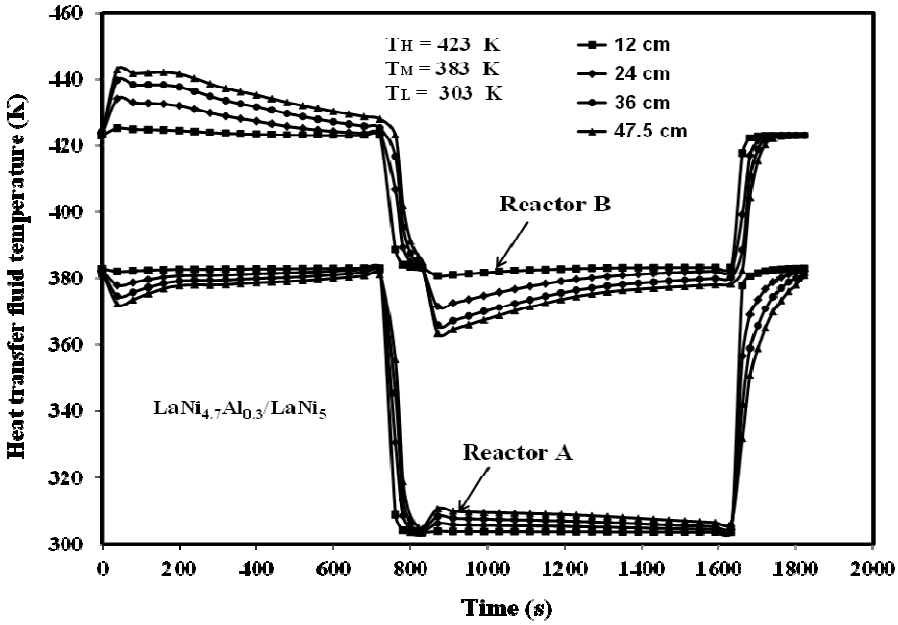

Fig. 7. Variations of HTF temperature at different.

5.5 Heat Interactions during the Operation of MHHT

The heat interaction between the HTF and the hydride bed during the four processes is illustrated in Figure 8. Initially (t = 0), the variation in the HTF temperature along the axial direction is zero. Due to the rapid absorption/desorption processes at the initial stage, the amount of heat is removed from/supplied to the reactor is very high. As the time progresses, the heat interaction is found to decrease gradually and becomes zero at the end of the process. This is due to the reason that owning to a large driving potential for heat and mass transfer between the coupled reactors, most of the hydrogen is transferred within few minutes from the beginning of the process. As the bed begins to absorb/desorb the hydrogen, the driving potential decreases gradually and hence, the hydrogen transfer rate also drops. Since, the rate of hydrogen exchange between the reactors decreases with time, the heat interaction is also found to be decrease. The amount of energy interaction from/to the reactor B is higher in comparison with the reactor A. This is due to the higher heat of formation of the hydride B. The heat transferred during the sensible heat transfer processes bc and da are much smaller than during the coupled heat and mass transfer processes ab and cd.

5.6 Effects of Hydride Bed Thickness and Thermal Conductivity on the Cycle Time and SHP

Figures 9 and 10 show the effects of hydride bed thickness and effective bed thermal conductivity on the cycle time and specific heating power (*SHP).* It is observed from Figure 9 that for a given bed thickness, the cycle time (t_{cy}) is found to decrease significantly

with hydride bed effective thermal conductivity (λ) up to about 8 W/m K. With further increase in λ, there is no significant change in the t_{cy}. For a given bed thickness of 10 mm, increase in λ from 2 W/mK to 8 W/mK reduces the cycle time by about 20 %. Effective thermal conductivity of the hydride bed can be improved from 0.4 W/mK (unmodified bed) to about 8 W/mK by either insertion of aluminium foam or integration of copper matrix. However, these techniques unnecessarily increase the thermal mass of the system.

Hence, a compromise should be obtained between the cycle time and the additional thermal mass. The effect of λ on the *SHP* is illustrated in Figure 10. Since, the SHP is sensitive on the cycle time, the increase in λ up to 12 W/mKis significant. The effect of bed thickness on t_{cy} and *SHP* are also seen in Figures 9 and 10. It is also seen from Figures 9 and 10 that for a given λ, thinner beds are preferable for shorter cycle time and higher *SHP*. For the given operating temperatures, the effects of above parameters on COP_{HT}, second law efficiency are negligible as the total heat transferred during a cycle remains the same.

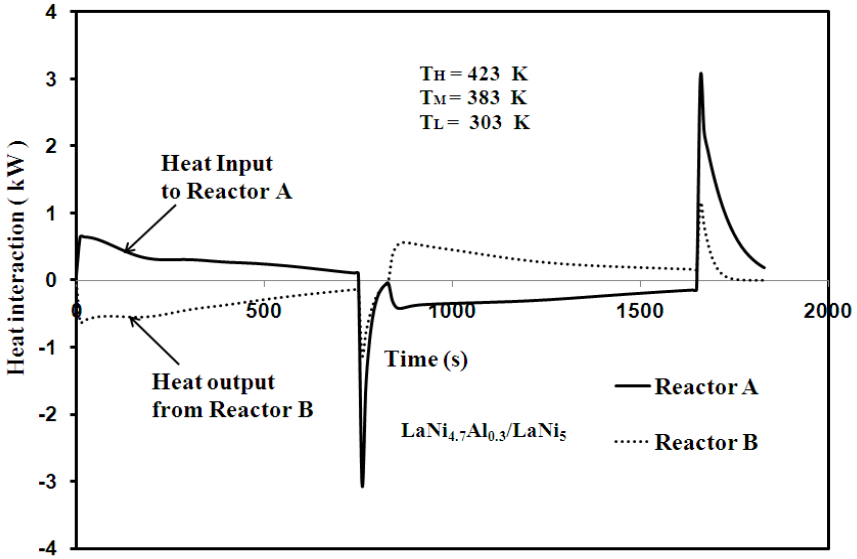

Fig. 8. Heat interactions during the operation of MHHT.

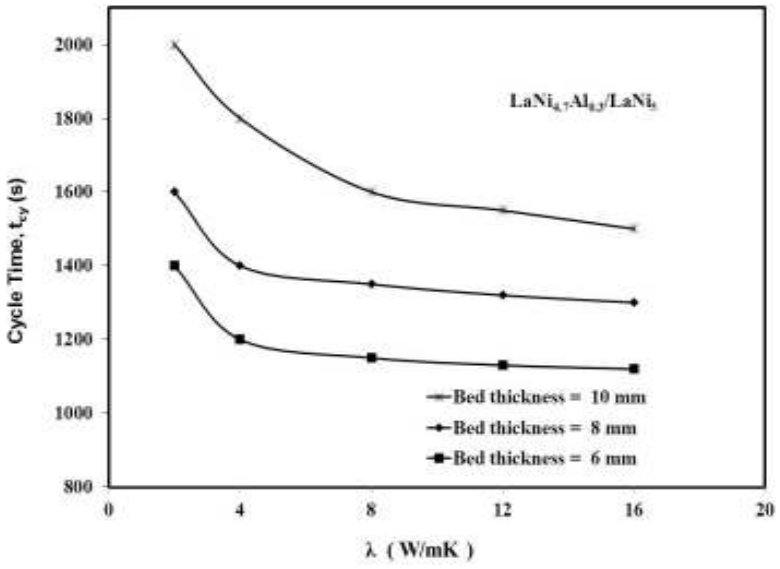

Fig. 9. Effect of bed thickness and thermal conductivity on cycle time.

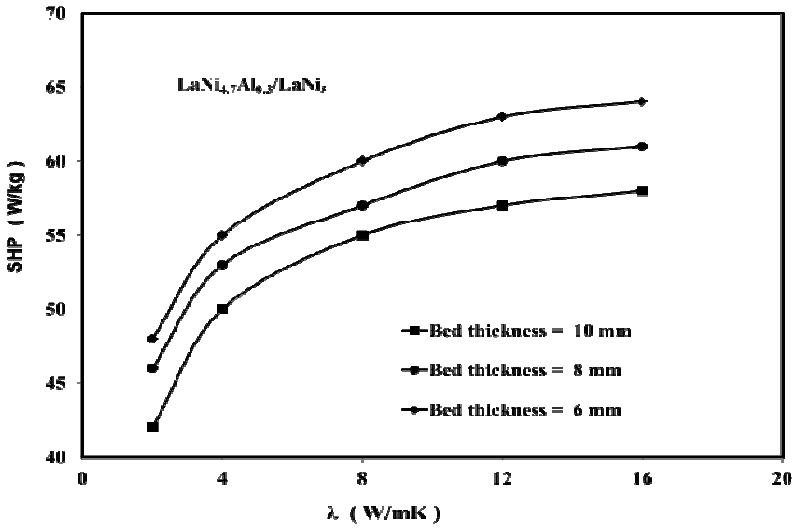

Fig. 10. Effect of bed thickness and thermal conductivity on *SHP*.

5.7 Effects of Heat Output and Heat Source Temperatures on COP_{HT} and SHP

The effects of the heat output temperature T_H and the heat source temperature T_M on the COP_{HT} and *SHP* are presented in Figures 11 and 12. For a given T_H, higher T_M's improve both the COP_{HT} and *SHP*. The increase in COP_{HT} with T_M is mainly due to the more amount of hydrogen exchange between the coupled reactors and the increase in *SHP* with T_M is due to the reduction in cycle time. While for a given T_M, higher T_H's reduce the driving potential for hydrogen transfer, resulting in higher cycle time and lesser hydrogen exchange between the paired reactors. As a result both the COP_{HT} and *SHP* decrease with T_H. At the operating conditions of T_M = 383 K and T_L = 303 K, the increase in T_H from 413 K to 428 K, reduce the COP_{HT} and the *SHP* by about 12.3 % and 22 %, respectively. The COP_{HT} and *SHP* are found to increase by about 8.75 % and 31 %, when the T_M is increased from 378 K to 393 K at T_H = 423 K and T_L = 303 K.

5.8 Effect of Heat Rejection Temperature on COP_{HT} and SHP

The effect of heat rejection temperature T_L on the COP_{HT} and the *SHP* at different T_M are illustrated in Figures 13 and 14. At higher T_L, the driving potential for mass transfer during the process cd is found to be less. As a result, the cycle time increases and hence, the *SHP* decrease. But the COP_{HT} increases slightly at higher T_L due to the reduction in the sensible heating requirement of the reactor A during the process da. However, the increase in T_L beyond 313 K yields an adverse effect on both COP_{HT} and *SHP* as the amount of hydrogen transfer during the process cd decreases considerably due to the reduction in hydride equilibrium pressure difference between the paired reactors A and B. It is seen from Figures 13 and 14 that the increase in T_L from 298 K to 313 K, improves the COP_{HT} marginally by about 2.5 %. But the reduction in *SHP* is about 5 %.

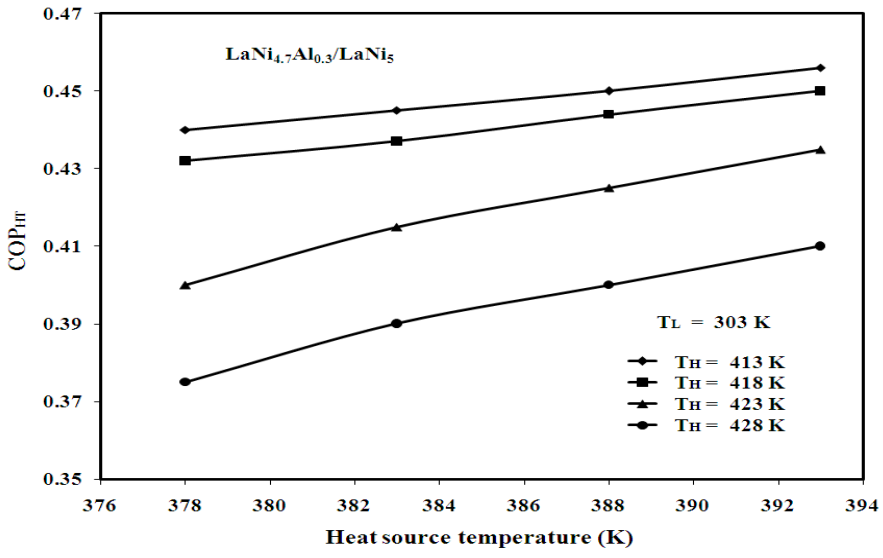

Fig. 11. Effect of heat output and heat source temperatures on COP_{HT}.

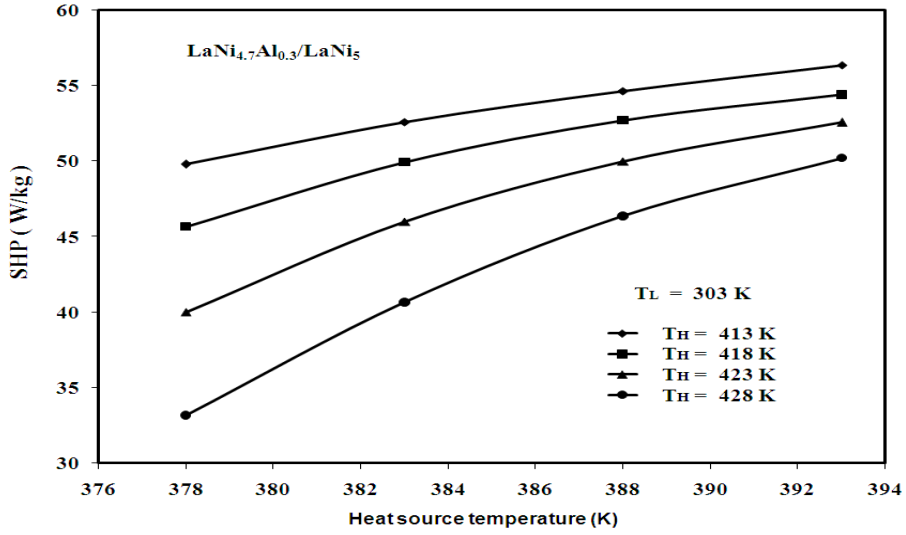

Fig. 12. Effect of heat output and heat source temperatures on *SHP*.

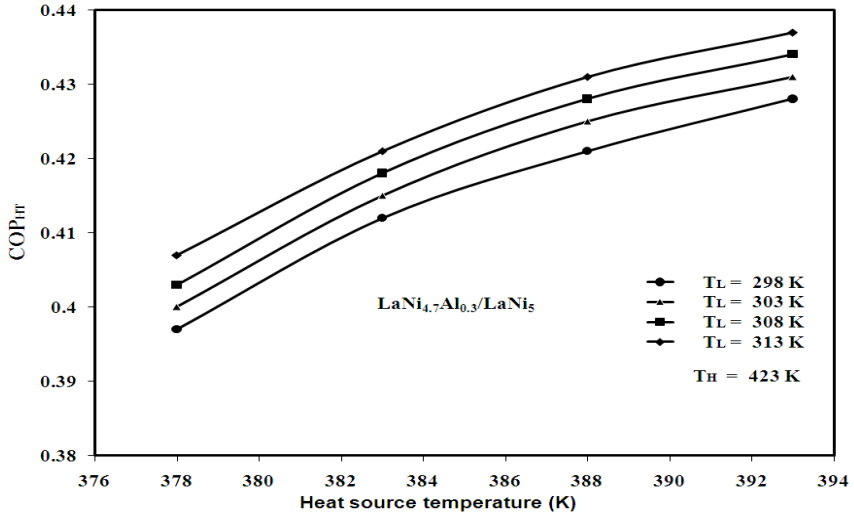

Fig. 13. Effect of heat source and heat rejection temperatures on COP_{HT}.

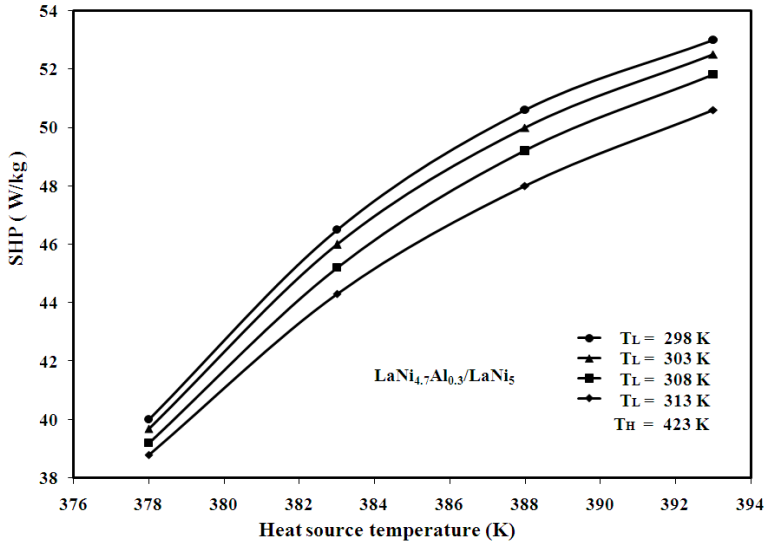

Fig. 14. Effect of heat source and heat rejection temperatures on *SHP*.

5.9 Effect of Heat Source and Heat Rejection Temperatures on η_E

Figure 15 shows the effects of heat source temperature T_M and heat rejection temperature T_L on the second law efficiency (η_E) of the MHHT. For a given T_H and T_L, η_E is found to decrease marginally with T_M. As explained in Figure 11 that the COP_{HT} increases with T_M but at the same time the improvement in COP_{Carnot} more than the increase in COP_{HT} with T_M. Since the η_E is ratio of COP_{HT} and COP_{Carnot}, the η_E is found to decrease by about 9.7 % when the T_M is increased from 378 K to 393 K. It is noted that for a given T_M = 383 K and T_H = 423 K the η_E increases by about 4.6% when the T_L is increased from 298 K to 313 K. This is due to the fact that higher T_L improves the COP_{HT} but reduces the COP_{Carnot} slightly. As a net result, the η_E increases with T_L.

5.10 Effect of Heat Output Temperature on η_E

The effect of heat output temperature T_H on the second law efficiency (η_E) at different T_M is illustrated in Figure 16. For a given heat source and heat rejection temperatures, the increase in heat output temperature decreases the COP_{HT}, but marginally increases the COP_{Carnot}. As a result, second law efficiency (η_E) decreases as the heat output temperature increases. For a given T_M = 378 K and T_L = 303 K, the η_E is found to decrease by about 4.4 % when the T_H is increased from 413 K to 428 K.

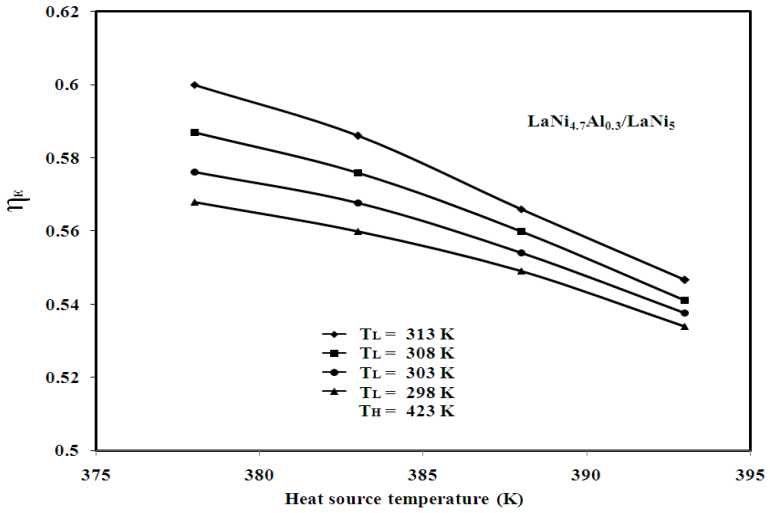

Fig. 15. Effect of heat source and heat rejection temperatures on η_E.

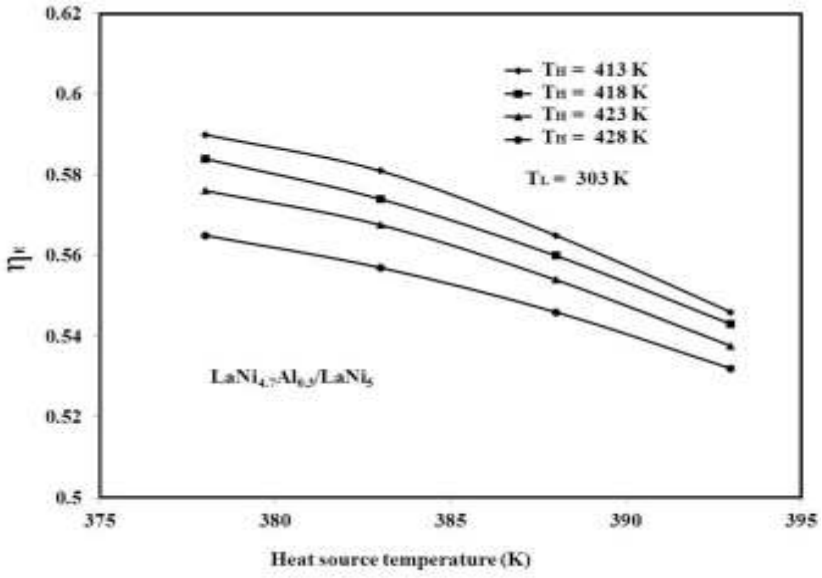

Fig. 16. Effect of heat output and heat source temperatures on η_E.

6. CONCLUSIONS

A thermal model for predicting the performances of a single-stage metal hydride based heat transformer (MHHT) is presented. Numerical results are compared with the experimental data reported in the literature, and a good agreement is found between them. The effects of heat output, heat source and heat rejection temperatures

on the system performances in terms of COP_{HT}, *SHP* and η_E are investigated. The cycle time of the non-isothermal wall convective temperature boundary condition is higher by about 3 min. compared to that of the isothermal wall convective temperature boundary condition.

For a given bed thermal conductivity of 4 W/mK, reducing the hydride bed thickness from 10 mm to 6 mm decreases the cycle time by about 30 %. The COP_{HT} and *SHP* of the MHHT are found to be 0.415 and 46 W/kg of alloy, respectively at the optimum value of operating temperatures viz., T_H = 423, T_M = 383 and T_L = 303 K. The COP_{HT} and *SHP* are found to increase by about 8.75 % and 31 %, when the T_M is increased from 378 K to 393 K and however, the increase in T_L from 298 K to 313 K, improves the COP_{HT} marginally only by about 2.5 %. But the reduction in *SHP* is about 5 %. The increase in T_H from 413 K to 428 K, reduce the COP_{HT} and the *SHP* by about 12.3 % and 22 %, respectively at the operating conditions of T_M = 383 K and T_L = 303 K. For a given T_M = 383 K and T_H = 423 K, the η_E increases by about 4.6 % when the T_L is increased from 298 K to 313 K.

NOMENCLATURE

A	Activation energy, J/mol H_2
Abs	Absorption
C_p	Specific heat, J/kg-K
Des	Desorption
h	Over all heat transfer coefficient, W/m^2-K
K	Permeability, m^2
m	Mass flux of hydrogen, kg/m^3-s
m_f	Mass flow rate of the heat transfer fluid, kg/s
M_g	Molecular weight of hydrogen, kg/kmol
n	Number of moles of hydrogen, mol
P	Pressure, bar
Q	Heat interaction, W
R	Reaction rate constant, s^{-1}
r_o	Outer radius of the reactor, m
R_u	Universal gas constant, J/mol-K
t	Time, s
T	Temperature, K
u	Velocity, m/s
V	Volume, m^3
X	Hydrogen concentration, (H/M ratio)
Z	Length of the reactor, m

Greek symbols

ε	Porosity
β	Hysteresis factor
ΔH	Enthalpy of reaction, J/mol H_2
ΔS	Entropy of reaction, J/mol H_2-K
ν_g	Kinematic viscosity, m^2/s
λ	Thermal conductivity, W/m-K
φ, φ_o	Slope factors
μ_g	Dynamic viscosity, kg/m-s
ρ	Density, kg/m^3

Subscripts

a	Absorption
A	Low temperature reactor
B	High temperature reactor
d	Desorption
e	Effective
eq	Equilibrium
f	Fluid, Final
fi	Heat transfer fluid inlet
fo	Heat transfer fluid outlet
g	Gas
i	inner
m	Metal
max	Maximum
min	Minimum
P	Connecting tube
ss	Saturation solid

REFERENCES

[1] Werner R. and M. Groll. 1991. Two-stage metal hydride heat transformer laboratory model: results of reaction test beds. *Journal of Less-Common Metals* 172:1122-1129.

[2] Suda S., Komazaki Y., Narasaki H. and Uchida, M., 1991. Development of a double-stage heat pump: Experimental and analytical survey. *Journal of Less-Common Metals* 172-174:1092-1110**.**

[3] Isselhorst A. and M. Groll. 1995. Two-stage metal hydride heat transformer laboratory model. *Journal of Alloys and Compounds* 231:888-894.

[4] Willers E. and M. Groll. 1999. The two-stage metal hydride heat transformer. *International Journal of Hydrogen Energy* 24:269-276.

[5] Kang B. and A. Yabe. 1995. Performance analysis of a metal-hydride heat transformer for waste heat recovery. *Journal of Applied Thermal Engineering* 16:677-690.

[6] Ram Gopal M. and S.S. Murthy. 1995. Prediction of metal hydride heat transformer performance based on heat transfer and reaction kinetics. *Industrial and Engineering Chemistry Research* 34:2305-2313.

[7] Bala Kumar M., Murthy S.S., Krishna Murthy M.V. and Sastri M.V.C., 1995. A comparative thermo dynamic study of metal hydride heat transformers and heat pumps. *Heat Recovery Systems and CHP* 5:527-534.

[8] Sun D.W. and M. Groll. 1992. Selection of alloys and their influences on the operation of a two stage metal hydride heat transformer. *Heat Recovery Systems and CHP* 12:49-55.

[9] George J.M. and S.S. Murthy. 1993. Experiments on a vapor absorption heat transformer. *International Journal of Refrigeration* 16:107-119.

[10] Yang F.S., Zhang Z.X., Wang G.X., Bao Z.W., Costa J.C.D. and Rudolph V., 2011. Numerical study of a metal hydride heat transformer for low-grade heat recovery: simulation of a MH heat transformer. *Journal of Applied Thermal Engineering* 31:2749-56.

[11] Yang F.S., Zhang Z.X. and Bao Z.W., 2012. An extensive parametric analysis on the performance of a single-stage metal hydride heat transformer.

International Journal of Hydrogen Energy 37:2623–34.

[12] Ni J. and H. Liu. 2007. Experimental research on refrigeration characteristics of a metal hydride heat pump in auto air-conditioning. *International Journal of Hydrogen Energy* 32:2567–72.

[13] Nishizaki T., Miyamoto K. and Yoshida K., 1983. Coefficients of performance of hydride heat pumps. *Journal of Less-Common Metals* 89:559–66.

[14] Mayer U., Groll M. and Supper W., 1987. Heat and mass transfer in metal hydride reaction beds: experimental and theoretical results. *Journal of Less-Common Metals* 131:235–44.

[15] Jemni A. and B.S. Nasrallah. 1995. Study of two-dimensional heat and mass transfer during absorption in a metal–hydrogen reactor. *International Journal of Hydrogen Energy* 20:43–52.

[16] Muthukumar P., Linder M., Mertz R. and Laurien, E., 2009. Measurement of thermodynamic properties of some hydrogen absorbing alloys. *International Journal of Hydrogen Energy* 34:1873-1879.

[17] Muthukumar P. and S.V. Ramana. 2009. Numerical simulation of coupled heat and mass transfer in metal hydride based hydrogen storage reactor. *Journal of Alloys and Compounds* 472:466-472.